

Redirecting the Route: Monocyte-Mediated Delivery of oHSV-1 Across a Human BBB-on-chip Model

Sara Micheli[#], Alberto Reale[#], Alessandra Rossetto, Cristina Parolin, Fabio Mammano, Arianna Calistri, Elisa Cimetta**

S. Micheli, E. Cimetta

Department of Industrial Engineering, University of Padua, Padua, Italy and

Fondazione Istituto di Ricerca Pediatrica Città della Speranza, Padua, Italy

elisa.cimetta@unipd.it

A. Reale, A. Rossetto, C. Parolin, A. Calistri

Department of Molecular Medicine, University of Padua, Italy

arianna.calistri@unipd.it

F. Mammano

Department of Physics and Astronomy “G. Galilei”, University of Padua, Padua, Italy and

CNR Institute of Biochemistry and Cell Biology, Monterotondo, Rome, Italy;

#Those Authors contributed equally to the work

Abstract

Oncolytic viruses (OVs) that selectively replicate within cancer cells represent a promising therapeutic strategy for refractory or difficult-to-treat tumors such as Glioblastoma (GBM). In this study, we develop and validate a human microfluidic blood brain barrier (BBB) model to evaluate the potential of cell-based OVs delivery targeting the central nervous system. We demonstrate that circulating leukocytes (monocytes), serve as effective carrier cells for the delivery of a neuroattenuated strain of oncolytic herpes simplex virus type 1 (oHSV-1) to GBM. Human monocytes infected with oHSV-1 and perfused through the device successfully traverse the BBB and migrate toward human GBM spheroids, where they deliver the virus and initiate infection. Notably, monocyte-mediated oHSV-1 delivery does not result in infection of the BBB and remains effective even in the presence of anti-HSV-1 antibodies, commonly found in the general population. In contrast, free oHSV-1 virions infect BBB-resident cells en route to the tumor and are neutralized by circulating human immunoglobulins. These findings highlight the potential of monocyte-based oHSV-1 delivery as a targeted, immune-shielded strategy for GBM therapy.

1. Introduction

The blood–brain barrier (BBB) is a specialized anatomical structure composed of vascular endothelial cells, pericytes, and astrocytes that selectively filters molecules from the bloodstream into the central

nervous system (CNS).^[1] As such, the BBB poses a significant challenge for the pharmacological treatment of CNS diseases^[2] such as glioblastoma (GBM).^[3] GBM is the most common primary brain tumor in adults^[4] and carries a very dismal prognosis.^[5] Despite some progress with chimeric antigen receptor (CAR)-T cell therapies, immunotherapy remains largely ineffective against GBM.^[6,7] This is due to multiple factors including inactivation by the tumor microenvironment, target antigen heterogeneity, and limited trafficking across the BBB, often necessitating intraventricular administration.^[8,9]

Oncolytic viruses (OVs) are naturally occurring or engineered viruses that selectively replicate in cancer cells by exploiting deficiencies in antiviral defence pathways.^[10] These agents offer a multifaceted therapeutic approach that includes direct tumor lysis, immune activation, and gene delivery.^[11] While talimogene laherparepvec (T-VEC), an oHSV-1-based OV, is approved for melanoma,^[12] another oHSV-1 has recently been authorized in Japan for GBM following promising clinical trials.^[13] Effective OV delivery to GBM remains a challenge. Intracranial injection, although effective, is invasive and not easily repeatable. Moreover, GBM's invasive nature and tendency to recur in distant brain areas make localized therapy insufficient. Intravenous administration is hindered by the BBB and by neutralization of circulating virions, particularly in the case of HSV-1, due to widespread pre-existing immunity in the population.^[14] Carrier cells provide a potential solution. These include mesenchymal stromal cells (MSCs)^[15] and immune cells such as monocytes, which we previously identified as suitable carriers for oHSV-1.^[16] These cells can be loaded *ex vivo* with the virus and exploit their innate tumor tropism to facilitate OV delivery while evading immune detection. Replicating the BBB *in vitro* poses challenges due to its complex cellular architecture. While *in vivo* studies offer physiological insights, they are limited by interspecies differences, ethical constraints, and scalability.^[17,18] Traditional static *in vitro* models fall short due to lack of shear stress and incomplete cellular interactions.^[19,20] Researchers developed BBB-on-chip systems, which are microfluidic platforms designed in attempt to replicate physiological and functional aspects of the BBB *in vitro*.^[21] Microfluidic BBB devices offer numerous advantages for *in vitro* modeling, making them an ideal alternative to traditional systems.^[17] They are cost-effective to fabricate and provide flexibility in design, allowing to tailor the setup to specific experimental needs. These devices require fewer cells, increase efficiency and reduce materials consumption.^[22] By offering precise control over the microenvironment, microfluidic systems can more closely replicate the actual *in vivo* brain anatomy, including critical factors such as shear stress.^[23] The ability to measure relevant parameters such as BBB permeability in real time, enhances both the speed and accuracy of data collection, while improving paracellular barrier functions. Additionally, the transparent nature of the devices allows for easy cell inspection via microscopy. With the possibility of integrating co-culture models, these microfluidic devices offer a more realistic simulation of the cellular interactions that occur within the brain, further advancing the physiological relevance of BBB modeling.^[24,25] Overall, microfluidic BBB models provide a promising alternative to traditional *in vitro* cell cultures and animal experimentation, offering the potential for more accurate and realistic BBB modeling.

In this study, we designed a tri-compartmental BBB-on-chip model incorporating endothelial, astrocytic, and pericytic layers, connected to a tumor chamber with GBM spheroids. We used this platform to demonstrate that monocytes can successfully deliver oHSV-1 across the BBB to infect GBM spheroids, even in the presence of neutralizing antibodies.

2. Results and discussion

2.1 A microfluidic BBB-on-chip model allows growth of multiple cell types and BBB-like permeability

The BBB-on-chip was designed with a structure consisting of three distinct layers to replicate the BBB microenvironment and incorporate a 3D GBM tumor culture for advanced cancer modeling (**Figure 1**). Each compartment serves a specific role in mimicking the physiological interactions between the blood and brain regions. The apical compartment, highlighted in red in **Figure 1.A**, represents the blood-facing side of the BBB. This layer enables the perfusion of culture medium and soluble species, simulating blood flow above the barrier. Continuous perfusion creates dynamic conditions critical for evaluating the transport and permeability of molecules across the BBB. The membrane layer, shown in black in **Figure 1.A**, plays a fundamental role in mimicking the selective barrier properties of the BBB. The membranes used in this model are made of transparent polyester (PETE) with a 3 μm pore diameter. The basolateral compartment, marked in yellow in **Figure 1.A**, represents the brain-facing side of the BBB. This compartment includes a tumor area composed of three microwells designed to accommodate 3D spheroids (red dashed box in **Figure 1.B**). The inclusion of the tumor compartment provides a physiologically relevant microenvironment to study tumor-BBB interactions, drug penetration, and spheroid behavior under perfused conditions.

Stable co-culture within the BBB-on-chip follows an optimized sequential seeding protocol to ensure the proper attachment and viability of all cell lines. Astrocytes and pericytes are first seeded on the basolateral side of the porous PETE membrane and then incubated overnight to facilitate adhesion. The following day, human umbilical vein endothelial cells (HUVECs) are seeded on the apical side to complete the BBB structure. Live/Dead assay results, presented in **Supplementary Figure S.1**, demonstrate successful attachment and high viability of all cell types on their respective side of the PETE membrane. These findings confirm that the seeding protocol and microenvironment within the BBB-on-chip are suitable for the growth and maintenance of the three-culture model.

Based on the results of numerical simulations, the cell culture medium perfusion flow rate through the blood side (Inlet/Outlet 2 in **Figure 1.B**) is set to 30 $\mu\text{L}/\text{min}$, corresponding to a shear stress at the bottom wall of ~ 7 dyne/cm^2 (see **Supplementary Figure S.2** for additional details). This value falls within the physiological shear stress range reported in the literature for blood vessels, which is between 3-25 dyne/cm^2 ^[26] and plays a critical role in maintaining BBB integrity and function. Physiological shear stress levels are also essential for regulating endothelial cell function, promoting barrier tightness, and facilitating proper nutrient and waste exchange.

After seeding, the maturation of the barrier in the microdevices was monitored over the course of 7 days, performing daily Transendothelial Electrical Resistance (TEER) measurements using a voltohmmeter (**Figure 1.C**). TEER values progressively increase over time, peaking approximately at 340 Ωcm^2 on day 7, indicating the successful formation and maturation of the barrier, consistently with available literature data for comparable on-chip systems.^[27]

After 7 days of perfused culture, the identity of cells growing on both sides of the membrane was confirmed by immunofluorescence. Specifically, we detected platelet and endothelial cell adhesion molecule 1 (PECAM, or CD31) and zonula occludens-1 (ZO-1) in the endothelial layer of the membrane. Both proteins are involved in endothelial cell junctions and ZO-1 has a prominent role in the formation of tight junctions, which are fundamental for BBB function. On the brain side of the barrier, we detected glial fibrillary acidic protein (GFAP), which is a widely used marker for astrocytes (**Figure 1.E**). Astrocytes play a critical role in maintaining BBB integrity by regulating tight junction formation, providing metabolic support, and modulating the selective permeability of

the barrier.^[28] Combined with the observed TEER increase, these results confirm the successful recreation of a functional BBB-like barrier within the microdevices.

We also tested the ability of our BBB model to restrict molecular diffusion using FITC-conjugated dextrans in a permeability assay. Dextrans of different molecular weights (40, 70, and 150 kDa) are perfused through the apical (blood channel) side of the device at a flow rate of 5 μ L/min. Fluorescence intensity is monitored in the tumor area across the three microwells using a fluorescence microscope with a 488 nm filter, and mean intensity values from specific regions of interest (ROI) are quantified with ImageJ software. To address the role of each cell type in determining the physiological compliance of the barrier after 7 days of perfused culture, we tested the permeability in: *i.* control devices without cells, *ii.* devices seeded with a HUVECs monolayer only, and *iii.* in the complete BBB model incorporating HUVECs, astrocytes, and pericytes. Representative permeability values are shown in **Figure 1.D** and demonstrate a clear correlation between dextran molecular weight and diffusion resistance. Dextrans with higher molecular weights (70 and 150 kDa) exhibit slower accumulation in the microwells across all experimental conditions, indicating increased difficulty in crossing the barrier. Control devices without cells show the highest permeability. In contrast, devices with a HUVEC monolayer exhibit significantly reduced permeability, which further decreases with the addition of astrocytes and pericytes. These findings importantly confirm that the incorporation of astrocytes and pericytes enhances the barrier's selectivity, more closely mimicking the tight junctions and restrictive properties of the *in vivo* BBB. The observed decrease in permeability aligns with the expected physiological role of these cell types in regulating molecular transport and maintaining BBB integrity.

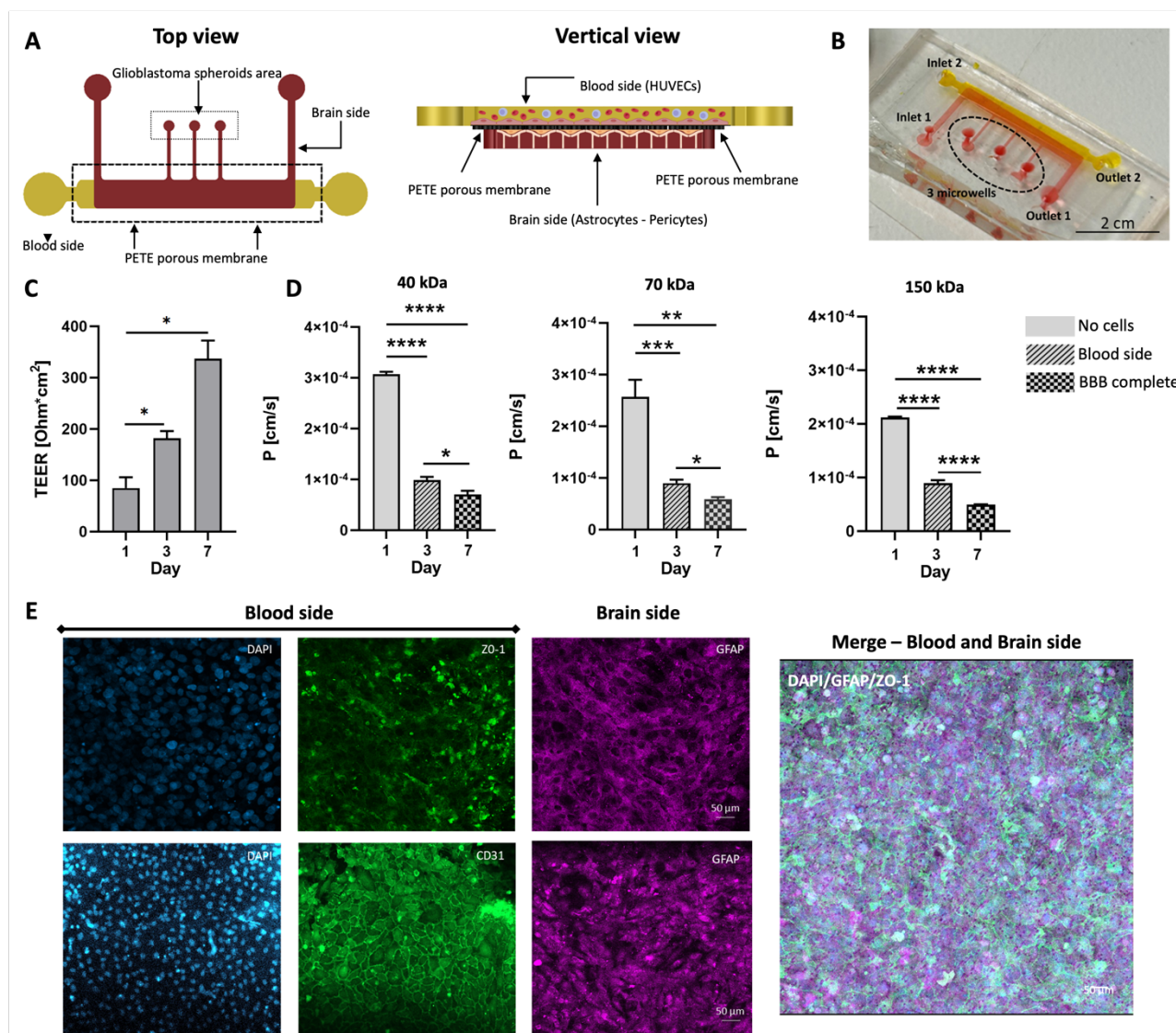


Figure 1. Microfluidic BBB-on-chip design and validation. **A.** Schematic representation of the BBB-on-chip, seeded with endothelial cells on the blood side and pericytes and astrocytes on the brain side, equipped with three microwells for 3D glioblastoma spheroid culture (glioblastoma spheroids area). **B.** Photograph of the assembled BBB-on-chip showing the upper channel (yellow) mimicking the vascular compartment and main perfusion conduit, and the lower channels (red) leading to the tumor compartment (scale bar = 2 cm). **C.** Transendothelial electrical resistance (TEER) measurements recorded daily across membrane interposed between the upper and lower channels and supporting the BBB. **D.** Permeability coefficients calculated from the diffusion of 40, 70, and 150 kDa FITC-dextran through the assembled BBB-on-chip in the following conditions: i. Control (membrane without cells), ii. Blood side (membrane + HUVECs endothelial monolayer), and iii. BBB (membrane with the three-culture of HUVECs on the blood side and pericytes and astrocytes on the brain side). **E.** ZO-1 and CD31 (green) are expressed on the blood-side compartment, confirming the formation of a functional endothelial barrier. GFAP (magenta) is localized on the brain-side compartment indicating proper astrocyte distribution. DAPI staining is shown only for the blood-side images, highlighting nuclei of endothelial cells. The merged image illustrates the compartmentalized organization of the BBB model, with distinct localization of endothelial and astrocytic markers, supporting the structural and cellular integrity of the reconstructed BBB. Scale bar = 50 μm . Values are expressed as median \pm SEM from at least 3 independent experiments. * $p < 0.05$, ** $p < 0.01$ and *** $p < 0.001$ vs control.

2.2 THP-1 cells transmit oHSV-1-mCherry to U87-derived spheroids, with infection leading to decreased viability in cancer cells

The growth and morphological characteristics of spheroids derived from human GBM U87 cells (U-87 MG, ATCC) are monitored over the course of 7 days. Brightfield images are captured with optimal contrast and analyzed using AnaSP software to quantify parameters such as equivalent diameter,

solidity, compactness and sphericity index (SI). The equivalent diameter of the spheroids increases from approximately 200 μm on day 2 to 700 μm on day 7, with some growing up to 800 μm (**Figure 2.A**). Solidity also increases over time, correlating with shape regularity, while compactness decreases due to growth-related effects. The maintenance of a spherical shape is confirmed by a stable SI around 1 throughout the observation period. **Figure 2.B** reports representative images for Phalloidin/DAPI staining and Live/Dead assay at day 7. To capture the 3D structure of the spheroid, sequential images focus on the outer (shell) and inner (core) sections. Phalloidin/DAPI staining shows well-structured actin filaments and organized nuclei, reflecting proper cellular architecture and spatial arrangement within the spheroids. The Live/Dead assay demonstrates consistent high cell viability. To explore the potential use of monocytes as carrier cells for the systemic delivery of an HSV-1 based OV, we assess the ability of human monocytic THP-1 cells to transmit oHSV-1-mCherry infection to GBM spheroids in standard multiwell culture settings. U87-derived spheroids are co-cultured with *i.* uninfected THP-1 cells labeled with CellTracker™ Green (Invitrogen™, Thermo Fisher Scientific), *ii.* labeled THP-1 infected with oHSV-1-mCherry at the multiplicity of infection (MOI) of 3 plaque forming units (PFU)/cell, and *iii.* free oHSV-1-mCherry. Monitoring the spheroids over several days using confocal microscopy enables evaluation of the spreading of the viral infection via m-Cherry fluorescence visualization. Images in **Figure 2.C** are representative of GBM spheroids at day 7 post treatment with THP-1 monocytes labeled in green and infected with oHSV-1-mCherry. The fluorescence images illustrate the widespread distribution of oHSV-1-mCherry infected cells (red) and of the carrier THP-1 cells (green) within the GBM spheroids. The same tumor spheroids are subjected to a viability MTT assay to measure their viability. On day 7 post-infection (**Figure 2.D**), the viability of spheroids is significantly reduced both after infection with the free virus and after incubation with oHSV-1-mCherry infected THP-1 cells, indicating an active replication of the virus in cancer cells, independently from the way of administration. Overall, these findings support the feasibility of using monocytes as carrier cells for the delivery of oHSV-1 to GBM cells.

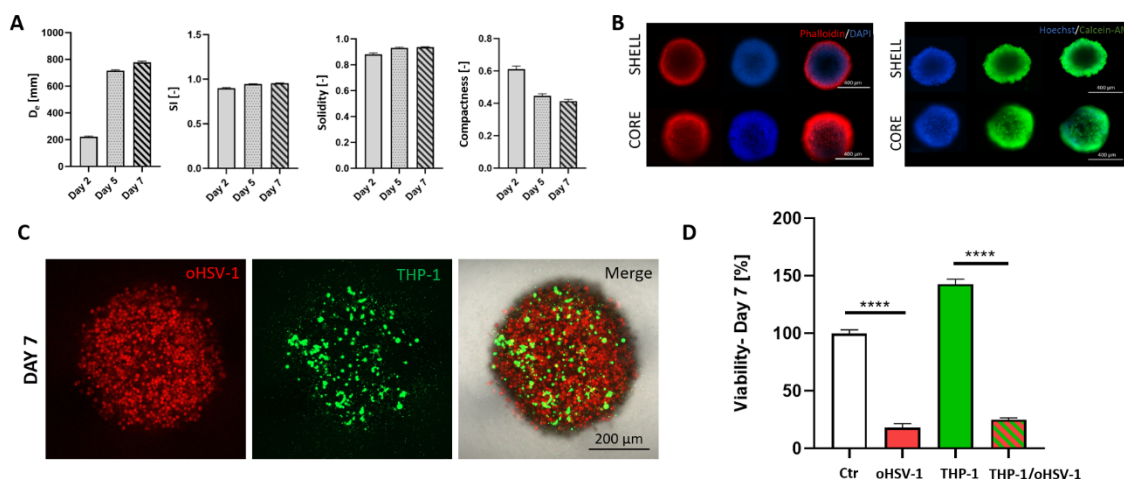


Figure 2. THP1 cells deliver oHSV-1 to U87 spheroids and the infection decreases tumor cells viability. **A.** Spheroids characterization: time course AnaSP measurements of: Equivalent diameter, Sphericity Index, Solidity, and Compactness. **B.** Representative phalloidin + DAPI staining (left) and Live/Dead assay (right) at day 7. F-actin filaments are marked red and cell nuclei blue, showing a correct distribution throughout the entire 3D structure. Cell viability is consistently high in both the shell and core of the spheroids, with cell nuclei marked in blue with Hoechst and cytoplasm of living cells marked in green with Calcein-AM. Scale bars 400 μm . **C.** U87-MG spheroids treated with THP-1 cells infected at MOI of 3 PFU/cell and labeled with CellTracker™ Green (500 cells/well). On day 7, the red signal of the encoded mCherry protein proves that viral infection propagated throughout the entire spheroid. **D.** MTT assay performed on day 7. Values are expressed as median \pm SEM from at least 3 independent experiments. **** $p < 0.0001$ vs control.

2.3 Perfused THP-1 cells loaded with oHSV-1-mCherry cross the BBB and transmit the viral infection to U87-derived tumor spheroids

The BBB-on-chip devices containing U87 GBM spheroids (one per microwell, for a total of three spheroids per device) are connected to the perfusion system on the blood side to deliver: *i.* THP-1 cells labeled with CellTracker™ Green and infected with oHSV-1-mCherry, *ii.* Naïve, labeled THP-1 cells, or *iii.* free oHSV-1-mCherry. Negative controls are also performed perfusing culture media only. Each device is maintained in perfused conditions and analyzed over several days using fluorescence microscopy to evaluate monocyte migration across the BBB and the transmission and spreading of the viral infection to the tumor spheroids.

First, green-labeled THP-1 monocytes can be detected in the apical compartment (blood side), and as early as after 24 hours successfully cross the BBB and are found in the microwells containing the U87 GBM spheroids (**Figure 3.A**). Focusing on the BBB (**Figure 3.B**), we observe infection, marked by red fluorescence, only when perfusing free oHSV-1-mCherry, proving that THP-1 cells shuttle the viral particles while minimally affecting the barrier. Analyzing the tumor compartment with the GBM spheroids (**Figure 3.C**), fluorescent signals are detected at the 24 hours timepoint, representative of THP-1 cells (green) and virally infected cells (red), further confirming successful crossing of the BBB and targeted migration towards the tumor spheroids. At the later timepoints of 48 and 72 hours, THP-1 cells infected with oHSV-1-mCherry penetrate the tumor spheroids, further transmitting the virus to cancer cells. Free oHSV-1-mCherry viral particles similarly reach the microwells and infect the spheroids, after infecting the cells of the barrier. The key findings from **Figure 3** can thus be summarized as follows. 1. Free oHSV-1-mCherry perfused through the blood side of the BBB-on-chip can infect and replicate within the BBB cells, potentially compromising their function. It is also conceivable that the attenuated virus would be eliminated in the presence of a competent immune system prior to reaching and crossing the barrier, a hypothesis that will be verified in the next sections. 2. When THP-1 monocytes are used as carriers for oHSV-1-mCherry, no infection of the BBB cells is observed, confirmed by the negligible red fluorescent signals. 3. Infected THP-1 cells successfully cross the BBB and transmit viral infection to tumor spheroids. Thus overall, monocyte-mediated delivery exerts a protective role, preserving the integrity and functionality of the BBB while facilitating targeted viral transmission to the tumor spheroids.

2.4 Human primary monocytes transmit oHSV-1-mCherry infection to GBM spheroids and cross the BBB in the microfluidic model

Building on the successful transmission of oHSV-1-mCherry infection by THP-1 cells to U87 GBM spheroids, we proceeded to use human primary monocytes from healthy donors as a more physiologically relevant source for carrier cells. Human primary monocytes isolated from validated buffy coats are labeled with CellTracker™ Green and loaded with oHSV-1-mCherry (MOI = 3 PFU/cell). To assess whether primary monocytes can effectively deliver their viral payload to tumor cells, we co-cultured oHSV-1-mCherry-loaded monocytes with U87 GBM spheroids in standard microwell conditions. Within 24 hours (**Supplementary Figure S.3A**), the monocytes successfully migrate toward and infiltrate the spheroids, accumulating at the tumor periphery and interior. By 48 hours, active viral replication is evident, and by day 7, red fluorescent signal from oHSV-1-mCherry is detected throughout the 3D tumor structure. At this point, spheroids exposed to loaded primary

monocytes exhibit a marked reduction in viability compared to untreated controls (**Supplementary Figure S.3B**).

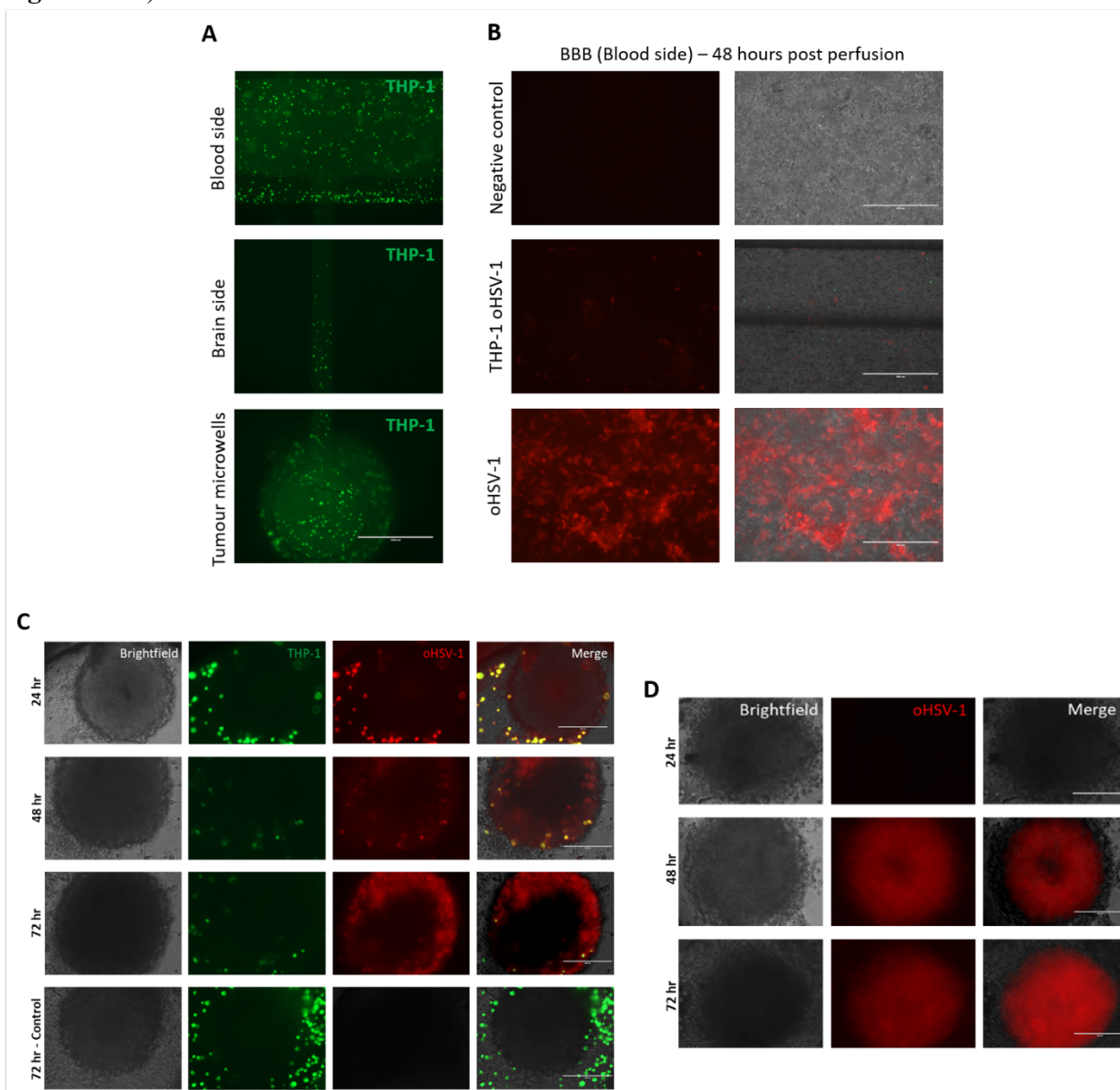


Figure 3. THP-1 cells cross the BBB-on-chip and deliver oHSV-1 to GBM tumor spheroids. **A.** The BBB-on-chip model is perfused with naïve THP-1 cells marked with CellTracker™ Green (5×10^5 cells/chip). After 24 hours, THP-1 cells crossing the BBB reach the GBM spheroids in the microwells of the tumor compartment. **B.** Representative images of the BBB after 48 hours of perfusion with: i. cell culture medium (negative control), ii. THP-1 cells infected with oHSV-1-mCherry, and iii. free virus. Scale bar: 200 μ m. **C.** U87 GBM spheroids within the BBB-on-chip perfused with THP-1 cells labeled with CellTracker™ Green and infected with oHSV-1-mCherry (MOI = 3 PFU/cell, 5×10^5 cells/chip), after 24, 48, and 72 hours. **D.** U87 GBM spheroids within the BBB-on-chip after perfusion with free oHSV-1-mCherry (1.5×10^6 PFU/chip) after 24, 48, and 72 hours. Scale bar: 200 μ m.

These findings demonstrate that, like THP-1 cells, human primary monocytes can deliver oHSV-1-mCherry with effective oncolytic activity. The ability of human primary monocytes loaded with oHSV-1-mCherry to cross the BBB and transmit viral infection to U87 GBM spheroids is then evaluated in the BBB-on-chip model. Human primary monocytes migrate through the device crossing the BBB as early as after 24 hours of perfusion through the blood side of the device. Green cells are detected in the bottom layer of the BBB, connecting channels, and in the microwells containing U87

GBM spheroids (**Figure 4.A**). Monocyte migration is enhanced in the presence of tumor spheroids, suggesting a signaling interplay between GBM cells, monocytes, and the BBB that could promote increased membrane permeability and immune cell recruitment toward the tumor niche. After 48 hours (**Figure 4.B**), human primary monocytes are observed adjacent to and within the U87 GBM spheroids in the tumor compartment, further confirming their targeting capability. At this stage, viral replication, indicated by red fluorescence, also becomes detectable. By day 5, the red fluorescent signal spreads throughout the 3D GBM spheroids (**Figure 4.B**), supporting the ability of human primary monocytes to deliver and transmit oHSV-1-mCherry infection to tumor cells.

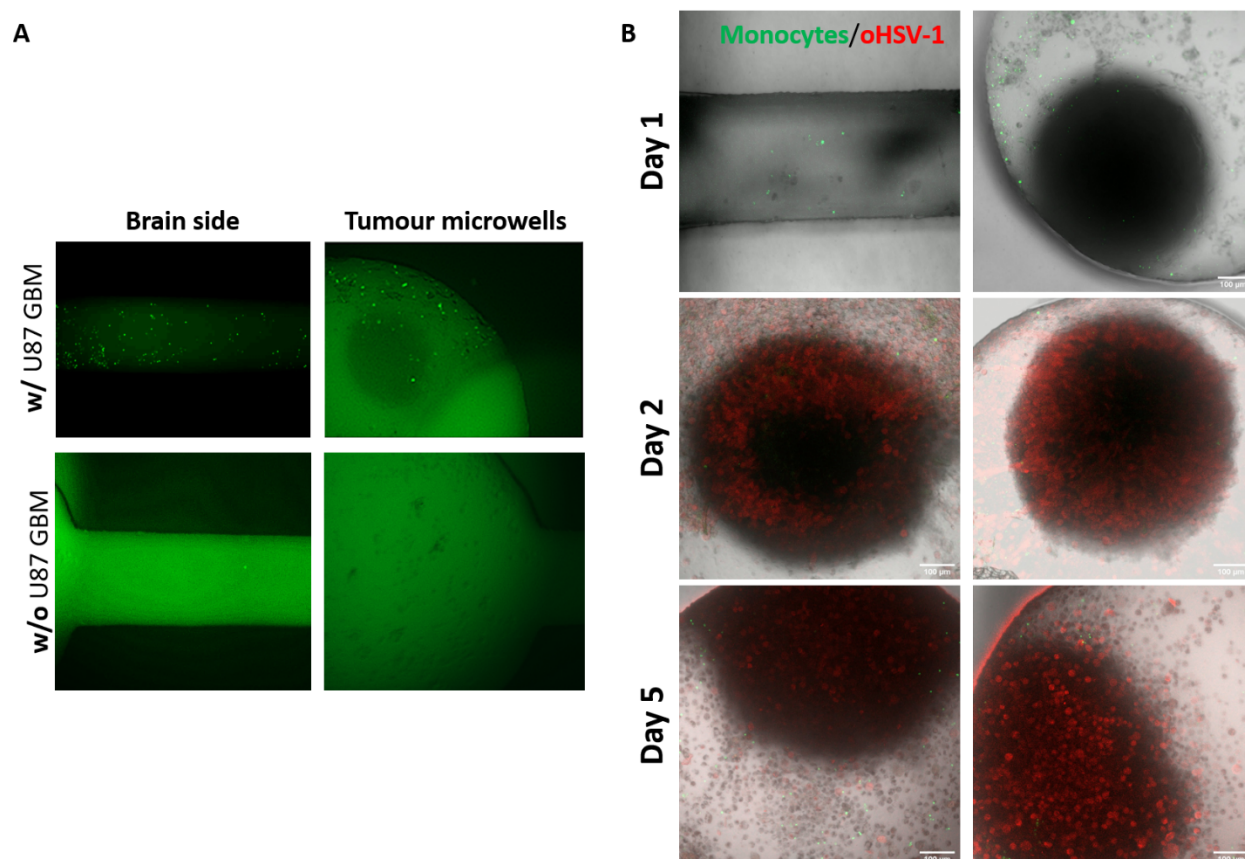


Figure 4. oHSV-1-loaded human primary monocytes cross the BBB-on-chip and deliver their viral cargo to GBM tumor spheroids. **A.** Human primary monocytes transmigration through the BBB increases in the presence of U87 GBM spheroids. Green fluorescent cells are more abundant in the basolateral compartment (brain side) and tumor microwells when spheroids are present (w/ U87-GBM). In contrast, devices without tumor spheroids (w/o U87-GBM) show limited to absent monocyte migration across the BBB. **B.** After 24 hours of perfusion, human primary monocytes loaded with oHSV-1-mCherry cross the BBB and reach the spheroids in the tumor compartment. Representative images of GBM spheroids at later timepoints after 2 and 5 days of loaded monocytes perfusion show progressively increasing red fluorescence signals indicating infection with the shuttled oHSV-1-mCherry.

2.5 Human primary monocytes cross the BBB and protect oHSV-1-mCherry from antibody neutralization, transmitting the viral infection to GBM tumor spheroids

Systemically administered free OV_s are limited by neutralization by pre-existing host antibodies, particularly for oncolytic agents based on viruses with high human seroprevalence, such as HSV-1.^[29]

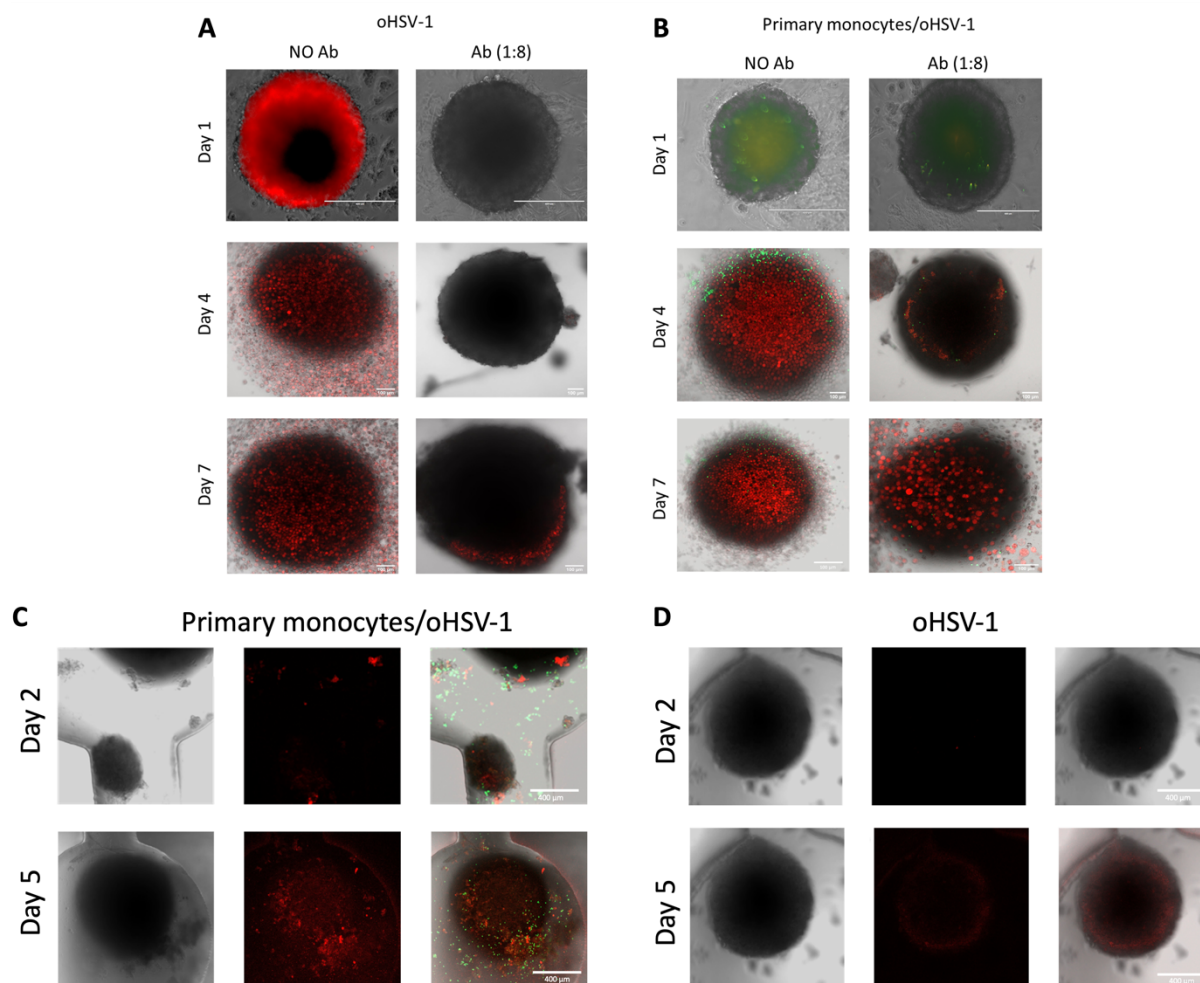


Figure 5. Human monocytes efficiently shield their oHSV-1 cargo from neutralizing human hyperimmune gamma globulins. **A.** Time course of GBM spheroids infected with free oHSV-1 mCherry (1.5×10^3 PFU/well) in static microwells with and without human hyperimmune IgGs (1:8 dilution). Scale bars 400 and 100 μm . **B.** Tumor spheroids treated with primary human monocytes infected with oHSV-1-mCherry (MOI = 3 PFU/cell, 5×10^3 cells/well) in static microwells with and without human hyperimmune IgGs (1:8 dilution). **C.** Primary human monocytes infected with oHSV-1 mCherry (MOI = 3 PFU/cell, 3×10^5 cells/chip) are perfused in the BBB-on-chip models in the presence of human hyperimmune IgGs (1:8 dilution) and monitored for 5 days confirming successful transmission of the infection. **D.** In a similar experimental setup, free virus (9×10^5 PFU/chip) is perfused in the BBB-on-chip in the presence of human hyperimmune IgGs (1:8 dilution) and monitored for 5 days confirming viral neutralization.

Carrier cells should shield OV's from immune recognition and thereby enhance their therapeutic efficacy. To evaluate if autologous monocytes can shield oHSV-1 from antibody-mediated neutralization, we chose a human hyperimmune IgG preparation that mimics the natural *in vivo* immune response by targeting a broad range of pathogens, including HSV-1. To better approximate the complexity of the human immune environment, we tested two conditions: a 1:4 dilution of hyperimmune IgG, fully neutralizing oHSV-1-mCherry replication in U87 GBM cells, and a 1:8 dilution, partially restricting viral spread but not completely inhibiting viral replication (Supplementary Figure S.4).

Figure 5 summarizes the key findings from GBM spheroids treated under both standard static and BBB-on-chip conditions. In static microwell cultures, control spheroids exposed to free oHSV-1-mCherry in the absence of antibodies show progressively increasing viral infection, with red fluorescence spreading throughout the entire spheroid by day 7. Conversely, the presence of hyperimmune IgGs (1:8 dilution) markedly restricts viral dissemination: no red fluorescent cells are

observed during the first 4 days, and only sparse fluorescence appears by day 7 (**Figure 5.A**). When tumor spheroids are treated with primary human monocytes loaded with oHSV-1-mCherry (labeled with CellTracker™ Green), viral replication is evident by day 4 in both control and IgG-treated conditions, and the infection continues to spread through day 7 (**Figure 5.B**). These results demonstrate that monocytes can effectively shield oHSV-1-mCherry from antibody-mediated neutralization in static culture. Moving to the *in vitro* BBB-on-chip model with GBM spheroids in the microwells of the tumor compartment, hyperimmune IgGs (1:8 dilution) are introduced into the perfusion medium alongside either free virus or OV-loaded primary human monocytes. After 48 hours of perfusion, green fluorescence is detected in the lower apical compartment of the chip, indicating that monocytes successfully crossed the barrier shuttling their viral cargo (**Figure 5.C**). At the same time point, red fluorescence confirmed viral transmission from monocytes to tumor cells. In contrast, chips perfused with free oHSV-1-mCherry exhibit no detectable red fluorescence, confirming viral neutralization in the presence of hyperimmune IgGs (**Figure 5.D**).

Conclusion

Previous studies, including our own, have shown that monocytes are not fully permissive to HSV-1 replication.^[16,30] However, in transwell-based systems, monocytes infected with oHSV-1- retain the ability to migrate toward tumor cells, where viral replication is enhanced, leading to selective oncolysis. Similar effects have been observed *in vivo* using the chorioallantoic membrane (CAM) model.^[16] In this study, we expanded on these findings by developing and applying a dynamic, physiologically relevant BBB-on-chip platform to investigate interactions among monocytes, oncolytic viruses (OVs), and the blood–brain barrier (BBB).

This model not only confirms the ability of both THP-1 and primary human monocytes to traverse the BBB but also demonstrates their potential to deliver and propagate viral infection to tumor cells within a controlled microenvironment that more closely mimics *in vivo* conditions. The key findings are summarized below.

- **Directed Monocyte Migration:** Monocytes preferentially migrate across the BBB in the presence of GBM spheroids, consistent with evidence that monocytes and tumor-associated macrophages (TAMs) are actively recruited to the glioma microenvironment through chemotactic cues (e.g., CD62L, CCL2, CXCL1, VEGF-A) and their corresponding receptors (e.g. CD62R, CCR2, CX3CR1, and VEGFR1).^[31]
- **Tumor-Triggered Viral Replication:** Infected monocytes do not release the virus en route nor infect BBB-resident cells. However, upon reaching GBM spheroids, viral replication is initiated, leading to robust infection and tumor cell death—comparable to direct free-virus treatment. These findings support the feasibility of using monocytes as safe, efficient viral carriers. Notably, monocyte differentiation triggered by tumor contact may enhance HSV-1 permissiveness, as suggested by previous reports.^[30,32] Our model provides a platform to systematically investigate this hypothesis.
- **Immune Shielding:** oHSV-1 carried by monocytes is effectively protected from neutralizing antibodies. Even in the presence of hyperimmune IgGs, viral delivery and infection of GBM spheroids remain robust—unlike free virus, which is rapidly neutralized.
- **Localized Infection Control:** Monocytes restrict viral delivery to the tumor site, avoiding off-target infection of other cellular compartments, including the BBB itself.

Taken together, our results support the potential of autologous monocytes as a “Trojan horse” strategy for the systemic delivery of oncolytic viruses (Ovs) to glioblastoma (GBM). This approach offers a minimally invasive, immune-evasive, and targeted therapeutic alternative to intracranial injection, with important implications for patient compliance and clinical translation. Future studies will be essential to further optimize this method and evaluate its safety and therapeutic efficacy in preclinical and clinical settings.

3. Experimental Section

BBB-on-chip design and fabrication: The geometry of the BBB-on-chip was designed using AutoCAD® software, and the master mold was fabricated on a silicon wafer using standard photolithography.^[33] The microfluidic device was replica molded in polydimethylsiloxane (PDMS; Sylgard 184; Dow Corning, Midland, MI, USA) using soft lithography techniques.^[33] Briefly, PDMS pre-polymer (10:1 elastomer base to curing agent, wt/wt) was degassed and poured over the SU-8 (Microchem, Newton, MA, USA) patterned wafer to imprint the apical and basolateral geometries. After curing at 80 °C, for 1 hour, the inlets and outlets were created using a 1 mm diameter biopsy punch. A transparent polyester membrane (PETE, 3 µm pore size, 12 µm thickness, Sterlitech Corp, Kent, WA, USA) was sandwiched and bonded between the apical and the basolateral PDMS layers using a plasma cleaner (Harrick Plasma, Ithaca, NY, USA). The assembled BBB-on-chip devices were bound to glass coverslips via further plasma treatment and sterilized with 70% ethanol followed by UV exposure for 60 minutes.

BBB-on-chip cells seeding and culturing: Human umbilical vein endothelial cells (HUVECs), brain vascular pericytes (hBVPs), and immortalized astrocytes (hAs) were obtained from Innoprot (Derio, Spain). HUVECs were expanded in fibronectin-coated (FN, Innoprot, 1 mg/ml) 75 cm² flasks using Endothelial Basal Medium (P60104, Innoprot) supplemented with 5% fetal bovine serum (FBS, Innoprot), 1% penicillin-streptomycin (P/S, Innoprot), and 1% endothelial cell growth supplement (ECGS, Innoprot). hBVPs and hAs were cultured in poly-L-lysine-coated (PLL, Innoprot, 1 mg/ml) 25 cm² flasks using Pericyte and Astrocyte Basal Medium, respectively, supplemented with 2% FBS, 1% growth supplement, and 1% P/S solution. For BBB-on-chip seeding, the PETE membrane was coated for 24 hours with FN (blood side) and PLL (brain side), followed by three Phosphate Buffer Saline (PBS, Sial s.r.l., Rome, Italy) washes. hAs and hBVPs were seeded on the brain side at densities of 5x10⁵ and 1x10⁵ cells, respectively. After 6 hours of inverted incubation to favor cells adhesion to the PETE membrane, devices were placed upright and incubated for 24 hours with medium changes every 8 hours (medium 1:1 mix of hAs and hBVP media). HUVECs were seeded at 6x10⁶ cells/mL in the vascular channel (blood side) and incubated for 4 hours. Devices were then perfused at 30 µL/min using tubing connected to inlet/outlet ports. The perfusion medium was composed by 75% HUVEC medium and 25% (1:1) hAs/hBVP media (please see **Supplementary Figure S.5** for optimization details). Devices were cultured for 7 days to ensure the correct formation and maturation of the BBB before experimentation.

TEER measurements: TEER values were monitored over 7 days using a Millicell-ERS2 volt-ohm meter (Millipore, Merck, Rahaway, NJ, USA) with STX01 electrodes. TEER values correlate with BBB formation and maturation. Measurements were recorded by placing electrodes at the blood and

brain sides of the PETE membrane. Devices without served as blanks. TEER was calculated using the following formula (1).

$$TEER = (R - R_{blank}) * A \quad (1)$$

where A is the membrane area, R is the measured resistance in the seeded BBB-on-chip device, and R_{blank} is the resistance in the blank device.

Characterization of BBB permeability: Permeability was assessed using 40, 70, and 150 kDa Fluorescein isothiocyanate isomer-dextran (FITC-dextran, 0.5 mg/mL). Three experimental groups were used: no cells, endothelial-only, and complete BBB (triculture). On day 7, the devices were perfused with FITC-dextran through the blood channel at 5 μ L/min and imaged at three regions of interest (ROIs) on the brain side in correspondence of the three microwells. Permeability is determined using a standard reference method, and the Apparent permeability (P_{app}) and BBB-specific permeability (P_{BBB}) were calculated using equations (2) and (3).^[34]

$$P_{app} = \frac{C_{(t)}V}{C_0A\Delta T} \quad (2)$$

$$\frac{1}{P_{BBB}} = \frac{1}{P_{app}} - \frac{1}{P_0} \quad (3)$$

where $C_{(t)}$ is dextran concentration in the brain side, V is volume, C_0 is blood-side concentration, A is surface area, ΔT is the assay time, and P_0 is the permeability of the blank device.

Shear stress calculation and modeling: Computational Fluid Dynamics (CFD) simulations were conducted using COMSOL Multiphysics 6.1 to model shear stress in the blood-side channel. The simulation used a laminar flow model, incorporating geometry, meshing, and inflow boundary condition sweeps to achieve the desired shear stress level. The working fluid was modeled as incompressible Newtonian mimicking culture media.^[35,36] Calculated Reynolds numbers remained below 2000, confirming laminar flow conditions.

Immunofluorescence staining: Cells within the BBB-on-chip were analyzed via immunofluorescence staining for zonula occludens protein-1 (ZO-1), CD31, glial fibrillary acidic protein (GFAP) on day 7 of culture. For staining, cells were fixed on-chip using 4% paraformaldehyde (PFA, Sigma-Aldrich, Merck) in PBS, followed by permeabilization with 0.1% Triton X-100 (Sigma-Aldrich, Merck). Samples were then blocked at room temperature for 1 hour using PBS containing 5% bovine serum albumin (BSA, Sigma-Aldrich, Merck) and 0.1% Triton X-100. Subsequently, chips were incubated overnight at 4°C with primary antibodies diluted in PBS containing 5% BSA and 0.1% Triton X-100: mouse anti-CD31 (1:200, Proteintech Group, Inc, Rosemont, IL, USA), mouse anti-ZO-1 (1:50, Proteintech), and rabbit anti-GFAP (1:200, Proteintech). After washing, samples were incubated for 1 hour at room temperature with Coralite488-conjugated goat anti-mouse (1:800, Proteintech) and Coralite647-conjugated goat anti-rabbit (1:800, Proteintech) secondary antibodies in PBS with 5% BSA and 0.1% Triton-X100. Following additional washes, nuclei were counterstained with DAPI (Sigma-Aldrich, Merck) 1:1000 in PBS for 10 minutes. Finally, samples were mounted using 80% glycerol (Sigma-Aldrich, Merck) in Milli-Q water. Imaging is performed using a confocal microscope (LSM 700, Zeiss, Milan, Italy).

Spheroid formation and characterization: U87 glioblastoma cells (U-87 MG, ATCC HTB-14™) were maintained as monolayers in DMEM high glucose (Sial s.r.l.) supplemented with 10% FBS (Thermo Fisher Scientific, Waltham, MA, USA), 1% MEM non-essential amino acids (NEAA, Thermo Fisher Scientific) and 1% P/S (Sial s.r.l.), under standard cell conditions (37°C, 5% CO₂, humidified atmosphere). Media were refreshed every 2–3 days. Spheroids were generated from trypsinized monolayer cells, as previously described.^[37] Briefly, 200 µL of cell suspension containing 2×10^3 cells were seeded into each well of an Ultra-Low Attachment (ULA) 96-well round bottom plate (Corning®, Thermo Fisher Scientific) and centrifuged at 130 g for 10 minutes to promote aggregation. Spheroids were cultured for 7 days, with medium replenishment on day 4. Spheroid morphology and growth were monitored via brightfield imaging (Evos Imaging System, Thermo Fisher). Morphometric parameters, including size, solidity, and sphericity index (SI), were analyzed using AnaSP, an open-source software.^[38] On day 7, viability was assessed using a Live/Dead assay with Calcein-AM (1:1000, Sigma-Aldrich, Merck), Hoechst (1:500, Sigma-Aldrich, Merck) and Propidium Iodide (1:250, Thermo Fisher Scientific) in PBS. After replacing the culture medium with 100 µl of staining solution, spheroids were incubated for 30 minutes at room temperature in the dark and then imaged using a fluorescence microscope (Axio Imager M1, Zeiss). For cytoskeletal labeling, spheroids were fixed on day 7 with 4% PFA, permeabilized using 0.1% Triton X-100, and incubated with CoraLite594-conjugated Phalloidin (1:400, Proteintech) in PBS for 1 hour at room temperature. Samples were washed, stained with DAPI (1:100) in PBS for 20 minutes, washed again, and finally imaged using a Zeiss LSM 700 confocal microscope.

oHSV-1-mCherry production: oHSV-1-mCherry ($\Delta\gamma34.5/\Delta Us12/miRNA124/mCherry$ -oHSV-1) is an engineered oncolytic herpes simplex virus type 1 (oHSV-1) with a genomic backbone similar to the clinically approved T-VEC (talimogene laherparepvec). This construct contains deletions of the $\gamma34.5$ and *Us12* genes, which contribute to viral neuroattenuation, but lacks the two copies of the human GM-CSF gene present in T-VEC. Additionally, it bears an mCherry expression cassette inserted into the UL55-UL56 intergenic region. Further neuroattenuation is achieved by incorporating miR-124 target sequences downstream of the essential viral replication gene *UL29*, thereby restricting viral replication in mature neurons where miR-124 is expressed. This virus was obtained via bacterial artificial chromosome (BAC) mutagenesis, following previously described protocols.^[39] The starting material is a BAC containing the full-length genome of HSV-1 strain 17⁻, modified to include $\gamma34.5$ deletions and an eukaryotic cassette encoding for firefly luciferase within the UL55-UL56 intergenic region. This BAC was kindly provided by Beate Sodeik (Hannover Medical School, Germany). To reconstitute infectious virus, the modified BAC was transfected into 293T cells using Lipofectamine 2000™ (Invitrogen™, Thermo Fisher Scientific). Viral stocks were then amplified in green monkey kidney Vero cells and quantified via plaque titration assay on Vero cells, as previously reported.^[40]

Static infection of U87-MG spheroids with oHSV-1-mCherry transported by THP-1 cells: After 7 days of maturation, U87-MG spheroids were inoculated with the oncolytic herpes simplex virus type 1 (oHSV-1)-mCherry at a multiplicity of infection (MOI) of 3 plaque forming units (PFU)/cell. THP-1 cells (ATCC TIB-202™) were cultured in Roswell Park Memorial Institute (RPMI, Gibco) medium supplemented with 10% FBS (Thermo Fisher Scientific) and 1% P/S, under standard cell culture conditions. Prior to infection, THP-1 cells were labeled with CellTracker™ Green (C2925, Invitrogen™, Thermo Fisher Scientific) by incubation in serum-free RPMI containing the dye (1

$\mu\text{L/mL}$) for 20 minutes at 37°C . Following labeling, cells were centrifuged (at 300 g, 5 minutes), washed twice with PBS, and resuspended in serum-free RPMI. Cells were then infected with oHSV-1-mCherry by incubation for 60 minutes at 37°C . Post-infection, cells were pelleted, washed three times with PBS to remove extracellular virions and resuspended in DMEM supplemented with 10% FBS. Approximately 500 infected THP-1 cells were added to each spheroid-containing well. Viral spread was monitored over time using confocal microscopy by tracking mCherry fluorescence. In parallel, the metabolic activity of the spheroids was assessed via an MTT assay (Sigma-Aldrich, Merck), serving as a proxy for cell viability and proliferation. Briefly, at selected time points, individual spheroids were transferred to flat bottom 96-well plates containing 100 μL /well of fresh medium and 50 μL /well of MTT solution (5 mg/mL PBS). After a 4-hour incubation at 37°C in the dark, the resulting formazan crystals were solubilized with 50 μL /well of DMSO. Absorbance was measured at 560 nm using a Spark[®] Multimode Microplate Reader (Tecan Group Ltd., Männedorf, Switzerland), and viability was relative to untreated control spheroids.

Perfusion of THP-1 cells infected with oHSV-1-mCherry in the BBB-on-chip: Upon full maturation of the BBB structure within the microfluidic devices, at day 7 U87-MG spheroids were transferred from ULA plates into the microwells of the BBB-on-chip (one spheroid per microwell, three per device). THP-1 cells were labeled with CellTracker[™] Green and infected with oHSV-1-mCherry at a MOI of 3 PFU/cell, as previously described. After infection, cells were centrifuged (1000 g, 5 minutes), washed three times with PBS, and resuspended in 2 mL of DMEM supplemented with 10% FBS, yielding a final concentration of 2.5×10^5 cells per mL. Infected THP-1 cells were perfused into the blood-side inlet of the microfluidic device using 5 mL Luer lock syringes (BD PlastiPak[™], Sial s.r.l.) at a flow rate of 5 $\mu\text{L}/\text{min}$. Control conditions include perfusion of: *i.* non-infected THP-1 cells ($\sim 5 \times 10^5$ per device) labeled only with CellTracker[™] Green, and *ii.* free oHSV-1-mCherry, added directly to the perfusion medium in equivalent viral doses to those used for THP-1 infection.

Primary human monocytes isolation: Primary human monocytes were isolated from buffy coats derived from the peripheral blood of healthy donors, provided by the Transfusion Center of the University Hospital of Padua. No prior approval from an ethical committee is required, as samples are obtained as byproducts of routine blood draws without any additional intervention or burden to the donor and all samples are fully anonymized and handled in compliance with relevant data protection and bioethics regulations. All donors were screened to exclude HIV, HBV, HCV, and *Treponema pallidum* infections. Peripheral Blood Mononuclear Cells (PBMCs) were first separated via density gradient centrifugation using Ficoll-Paque[®] Plus (GE17-1440-03, Sigma-Aldrich, Merck), following the manufacturer's protocol. Briefly, the buffy coat was gently mixed by inversion (6–8 times), then diluted 1:1 with serum-free RPMI. A layer of Ficoll was carefully added to the bottom of a Falcon tube, and the diluted blood was layered on top without disturbing the gradient. The tubes were then centrifuged at 1000 g for 20 minutes. The resulting PBMC layer was carefully collected and transferred to a fresh tube.^[41] Next, cells underwent three washes with PBS, each followed by centrifugation at 1000 g for 8 minutes. A final wash at 800 g for 10 minutes removed residual platelets. Monocytes were then positively selected using the EasySep[™] Human CD14 Positive Selection Kit II (Stemcell[™] Technologies, Vancouver, Canada), according to the manufacturer's instructions.

Flow cytometry analysis for human primary monocytes: Following isolation, human primary monocytes were counted using a hemocytometer or an automated cell counter. To assess purity, 1×10^6 cells were resuspended in PBS and incubated with a fluorophore-conjugated anti-CD14 antibody (CD14V450, Becton Dickinson, Milan, Italy) for 30 minutes at 4°C in the dark. After incubation, cells were washed and resuspended in PBS. Samples were analyzed using a flow cytometer (FACS Canto II, Becton Dickinson) with gating applied to viable single cells. Monocyte purity was determined based on the percentage of CD14⁺ cells, with a threshold of $\geq 80\%$ indicating successful isolation.

Static and BBB-on-chip infection of U87-GBM spheroids with oHSV-1-mCherry transported by primary monocytes: The static infection of U87-GBM spheroids with human primary monocytes was performed according to the protocols described in the previous sections. Human primary monocytes, isolated from buffy coats, were infected with oHSV-1-mCherry (MOI = 3 PFU/cell) for 1 hour at 37°C. After infection, cells were labeled with CellTracker™ Green (diluted in serum-free RPMI) by incubating for 20 minutes at 37°C. Monocytes were then pelleted, resuspended in DMEM supplemented with 10% FBS, and added to pre-formed U87-MG tumor spheroids at a concentration of 5×10^3 cells per spheroid. For BBB-on-chip experiments, primary human monocytes were stained with CellTracker™ Green and infected with oHSV-1-mCherry at an MOI of 3 PFU/cell, as described above. Following infection, monocytes were resuspended in 2 mL of DMEM supplemented with 10% FBS to achieve a final concentration of 3×10^5 cells/mL. This suspension was loaded into 5 mL Luer-lock syringes and perfused through the blood-side inlet of the BBB-on-chip device at a constant flow rate of 5 μ L/min. Control conditions included: *i.* non-infected primary monocytes labeled only with CellTracker™ Green (3×10^5 cells per device), and *ii.* free oHSV-1-mCherry, both following the same perfusion protocol.

Experiments on antibody neutralization in static and BBB-on-chip conditions using infected primary monocytes: Following infection, human primary monocytes stained with CellTracker™ Green were resuspended in DMEM supplemented with 10% FBS and a 1:8 dilution of Human Gamma Globulin Control antibodies (IgG, Invitrogen, Thermo Fisher Scientific). A total of 5×10^3 monocytes were added to each U87 GBM spheroid, which was resuspended in 100 μ L of DMEM containing 10% FBS and 1:8 IgG. In parallel, U87-MG spheroids were directly infected with free oHSV-1-mCherry, using the same viral load used for infecting monocytes, in the presence of 1:8 diluted antibodies. Viral replication and spread within the tumor spheroids were monitored by confocal microscopy. Control spheroids, treated with either oHSV-1-mCherry-infected primary monocytes or free virus, were maintained in DMEM with 10% FBS in the absence of immunoglobulins. For BBB-on-chip studies, infected monocytes were resuspended in 2 mL of DMEM containing 10% FBS and a 1:8 dilution of human IgG. The cell suspension was then perfused into the device through the blood-side inlet. Spheroids within the BBB-on-chip were monitored over several days using confocal microscopy to assess differences in viral propagation in the presence of neutralizing antibodies, based on the delivery strategy of the oncolytic virus.

Statistical Analysis: Graphs were compiled using OriginPro® software, and statistical analyses were performed using GraphPad Prism. All graphical data represent the mean \pm standard error of the mean (SEM) from at least three independent experiments. Comparisons between multiple groups were conducted using one-way ANOVA, while comparisons between two groups were performed using

the Student's t-test. Statistical significance is indicated by asterisks, denoting differences between treated and control groups unless otherwise specified. * $p < 0.05$, ** $p < 0.01$, *** $p < 0.001$, **** $p < 0.0001$.

Supporting Information

Acknowledgements

This research project has received funding from the European Commission, ARACHNID project (ERC-2023-POC, id: 55008, CIME_UERI24_01) to E.C. and INFRAPLUS (Proposal number: 101131669, Proposal title: Enhancing and Evolving INFRAFRONTIER Disease Modelling Capacity to Enable Breakthrough Research) to F.M.; Fondazione Giovanni Celegghin Contro I Tumori Cerebrali to A.C.; Associazione Italiana per la Ricerca sul Cancro (AIRC IG 27797) to F.M.; University of Padova (PARO_FINA20_01) to C.P.

Conflict of Interest

The authors declare no conflict of interest.

Data Availability Statement

All original data are available at: <https://researchdata.cab.unipd.it/id/eprint/1544>

Keywords

BBB-on-chip, Glioblastoma spheroids, monocytes, oncolytic HSV-1

References

- [1] B. Obermeier, R. Daneman, R. M. Ransohoff, *Nat. Med.* **2013**, *19*, 1584.
- [2] R. Pandit, L. Chen, J. Götz, *Adv. Drug Deliv. Rev.* **2020**, *165–166*, 1.
- [3] K. H. Narsinh, E. Perez, A. F. Haddad, J. S. Young, L. Savastano, J. E. Villanueva-Meyer, E. Winkler, J. de Groot, *Curr. Neurol. Neurosci. Rep.* **2024**, *24*, 123.
- [4] T. Tykocki, M. Eltayeb, *J. Clin. Neurosci. Off. J. Neurosurg. Soc. Australas.* **2018**, *54*, 7.
- [5] H.-G. Wirsching, E. Galanis, M. Weller, *Handb. Clin. Neurol.* **2016**, *134*, 381.
- [6] R. Medikonda, G. Dunn, M. Rahman, P. Fecci, M. Lim, *J. Neurooncol.* **2021**, *151*, 41.
- [7] C. E. Brown, A. Rodriguez, J. Palmer, J. R. Ostberg, A. Naranjo, J. R. Wagner, B. Aguilar, R. Starr, L. Weng, T. W. Synold, V. Tran, S. Wang, A. Reik, M. D'Apuzzo, J. A. Ressler, Y. Zhou, M. Mendel, P. D. Gregory, M. C. Holmes, W. W. Tang, S. J. Forman, M. C. Jensen, B. Badie, *Neuro. Oncol.* **2022**, *24*, 1318.
- [8] D. M. O'Rourke, M. P. Nasrallah, A. Desai, J. J. Melenhorst, K. Mansfield, J. J. D. Morrisette, M. Martinez-Lage, S. Brem, E. Maloney, A. Shen, R. Isaacs, S. Mohan, G. Plesa, S. F. Lacey, J.-M. Navenot, Z. Zheng, B. L. Levine, H. Okada, C. H. June, J. L. Brogdon, M. V Maus, *Sci. Transl. Med.* **2017**, *9*, DOI 10.1126/scitranslmed.aaa0984.
- [9] B. D. Choi, E. R. Gerstner, M. J. Frigault, M. B. Leick, C. W. Mount, L. Balaj, S. Nikiforow,

- B. S. Carter, W. T. Curry, K. Gallagher, M. V Maus, *N. Engl. J. Med.* **2024**, 390, 1290.
- [10] S. J. Russell, K.-W. Peng, J. C. Bell, *Nat. Biotechnol.* **2012**, 30, 658.
- [11] A. Reale, A. Vitiello, V. Conciatori, C. Parolin, A. Calistri, G. Palù, *Infect. Agent. Cancer* **2019**, 14, 5.
- [12] R. M. Conry, B. Westbrook, S. McKee, T. G. Norwood, *Hum. Vaccin. Immunother.* **2018**, 14, 839.
- [13] T. Todo, H. Ito, Y. Ino, H. Ohtsu, Y. Ota, J. Shibahara, M. Tanaka, *Nat. Med.* **2022**, 28, 1630.
- [14] R. A. Ageeb, M. Harfouche, H. Chemaitelly, L. J. Abu-Raddad, *iScience* **2024**, 27, 110652.
- [15] A. Hadryś, A. Sochanik, G. McFadden, J. Jazowiecka-Rakus, *Eur. J. Pharmacol.* **2020**, 874, 172991.
- [16] A. Reale, L. Krutzke, M. Cadamuro, A. Vitiello, J. von Einem, S. Kochanek, G. Palù, C. Parolin, A. Calistri, *Int. J. Mol. Sci.* **2023**, 24, DOI 10.3390/ijms24119255.
- [17] M. A. Deli, G. Porkoláb, A. Kincses, M. Mészáros, A. Szecskó, A. E. Kocsis, J. P. Vigh, S. Valkai, S. Veszeka, F. R. Walter, A. Dér, *Lab Chip* **2024**, 24, 1030.
- [18] S. Reshma, K. B. Megha, S. Amir, S. Rukhiya, P. V Mohanan, *J. Drug Deliv. Sci. Technol.* **2023**, 80, 104174.
- [19] L. Cucullo, M. Hossain, V. Puvenna, N. Marchi, D. Janigro, *BMC Neurosci.* **2011**, 12, 1.
- [20] E. Jagtiani, M. Yeolekar, S. Naik, V. Patravale, *J. Control. Release* **2022**, 343, 13.
- [21] C. E. Staicu, F. Jipa, E. Axente, M. Radu, B. M. Radu, F. Sima, *Biomolecules* **2021**, 11, DOI 10.3390/biom11060916.
- [22] W. Bi, S. Cai, T. Lei, L. Wang, *Ageing Res. Rev.* **2023**, 87, 101921.
- [23] L. M. Griep, F. Wolbers, B. de Wagenaar, P. M. ter Braak, B. B. Weksler, I. A. Romero, P. O. Couraud, I. Vermes, A. D. van der Meer, A. van den Berg, *Biomed. Microdevices* **2013**, 15, 145.
- [24] J. Banerjee, Y. Shi, H. S. Azevedo, *Drug Discov. Today* **2016**, 21, 1367.
- [25] T. G. Schreiner, I. Creangă-Murariu, B. I. Tamba, N. Lucanu, B. O. Popescu, *Biomolecules* **2022**, 12, DOI 10.3390/biom12081136.
- [26] A. Kamiya, R. Bukhari, T. Togawa, *Bull. Math. Biol.* **1984**, 46, 127.
- [27] C. S. Lee, K. W. Leong, *Curr. Opin. Biotechnol.* **2020**, 66, 78.
- [28] M. Ohbuchi, M. Shibuta, K. Tetsuka, H. Sasaki-Iwaoka, M. Oishi, F. Shimizu, Y. Nagasaka, *Int. J. Mol. Sci.* **2024**, 25, DOI 10.3390/ijms25126496.
- [29] H. Bradley, L. E. Markowitz, T. Gibson, G. M. McQuillan, *J. Infect. Dis.* **2014**, 209, 325.
- [30] K. Linnavuori, T. Hovi, *J. Gen. Virol.* **1981**, 52, 381.
- [31] M. D. Caverzán, L. Beaugé, P. M. Oliveda, B. Cesca González, E. M. Bühler, L. E. Ibarra, *Brain Sci.* **2023**, 13, DOI 10.3390/brainsci13040542.
- [32] K. Linnavuori, T. Hovi, *Virology* **1983**, 130, 1.
- [33] Y. Xia, G. M. Whitesides, *Angew. Chem., Int. Ed. Engl.* **1998**, 37, 550.
- [34] B. Peng, Z. Tong, W. Y. Tong, P. J. Pasic, A. Oddo, Y. Dai, M. Luo, J. Frescene, N. G. Welch, C. D. Easton, H. Thissen, N. H. Voelcker, *ACS Appl. Mater. Interfaces* **2020**, 12, 56753.
- [35] W. Y. Chan, Y. Ding, J. Y. Tu, in *Proc. 7th Bienn. Eng. Math. Appl. Conf. EMAC-2005* (Eds: A. Stacey, B. Blyth, J. Shepherd, A.J. Roberts), **2007**, pp. C507--C523.
- [36] S. Micheli, P. Mocellin, M. Sorgato, L. Bova, E. Cimetta, *Biochem. Eng. J.* **2022**, 181, 108415.
- [37] V. Zingales, C. Piunti, S. Micheli, E. Cimetta, M.-J. Ruiz, *Foods* **2024**, 13, DOI 10.3390/foods13244167.
- [38] F. Piccinini, *Comput. Methods Programs Biomed.* **2015**, 119, 43.
- [39] B. K. Tischer, J. von Einem, B. Kaufer, N. Osterrieder, *Biotechniques* **2006**, 40, 191.
- [40] A. Vitiello, A. Reale, V. Conciatori, A. Vicco, A. Garzino-Demo, G. Palù, C. Parolin, J. von Einem, A. Calistri, *Biomedicines* **2024**, 12, DOI 10.3390/biomedicines12071577.

- [41] A. J. Ulmer, H. D. Flad, *J. Immunol. Methods* **1979**, 30, 1.